ACS APPLIED MATERIALS & INTERFACES
Research Article
www.acsami.org

Efficient Electrochemical CO_2 Conversion Powered by Renewable Energy

Douglas R. Kauffman,*[,†] Jay Thakkar,[†] Rajan Siva,[†] Christopher Matranga,[†] Paul R. Ohodnicki,[†] Chenjie Zeng,[‡] and Rongchao Jin[‡]

[†]National Energy Technology Laboratory, United States Department of Energy, Pittsburgh, Pennsylvania 15236, United States
[‡]Department of Chemistry, Carnegie Mellon University, Pittsburgh, Pennsylvania 15213, United States

Supporting Information

ABSTRACT: The catalytic conversion of CO_2 into industrially relevant chemicals is one strategy for mitigating greenhouse gas emissions. Along these lines, electrochemical CO_2 conversion technologies are attractive because they can operate with high reaction rates at ambient conditions. However, electrochemical systems require electricity, and CO_2 conversion processes must integrate with carbon-free, renewable-energy sources to be viable on larger scales. We utilize Au_{25} nanoclusters as renewably powered CO_2 conversion electrocatalysts with $CO_2 \rightarrow CO$ reaction rates between 400 and 800 L of CO_2 *per* gram of catalytic metal *per* hour and product selectivities between 80 and 95%. These performance metrics correspond to conversion rates approaching 0.8−1.6 kg of CO_2 *per* gram of catalytic metal *per* hour. We also present data showing CO_2 conversion rates and product selectivity strongly depend on catalyst loading. Optimized systems demonstrate stable operation and reaction turnover numbers (TONs) approaching 6×10^6 mol_{CO_2} $mol_{catalyst}^{-1}$ during a multiday (36 h total hours) CO_2 electrolysis experiment containing multiple start/stop cycles. TONs between 1×10^6 and 4×10^6 mol_{CO_2} $mol_{catalyst}^{-1}$ were obtained when our system was powered by consumer-grade renewable-energy sources. Daytime photovoltaic-powered CO_2 conversion was demonstrated for 12 h and we mimicked low-light or nighttime operation for 24 h with a solar-rechargeable battery. This proof-of-principle study provides some of the initial performance data necessary for assessing the scalability and technical viability of electrochemical CO_2 conversion technologies. Specifically, we show the following: (1) all electrochemical CO_2 conversion systems will produce a net increase in CO_2 emissions if they do not integrate with renewable-energy sources, (2) catalyst loading vs activity trends can be used to tune process rates and product distributions, and (3) state-of-the-art renewable-energy technologies are sufficient to power larger-scale, tonne *per* day CO_2 conversion systems.

Carbon Negative CO_2 Conversion

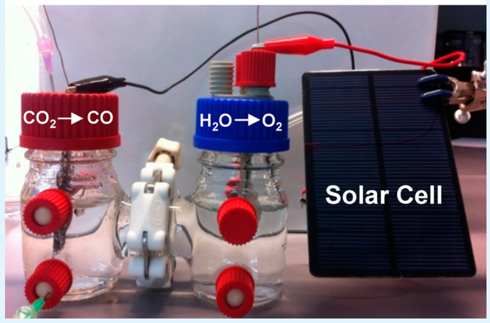

KEYWORDS: *electrocatalysis, CO_2 conversion, gold nanomaterials, renewable energy, catalysis, environmental*

INTRODUCTION

Greenhouse gas mitigation is one of today's most important scientific challenges. One promising approach for addressing these emissions involves catalytically converting waste CO_2 into industrially relevant chemicals.[1−14] This approach would reduce the carbon footprint associated with fossil fuels, provide new feedstocks for petrochemical production, and generate revenue to offset CO_2 capture and storage costs. Ultimately, CO_2 conversion can help establish a closed-loop, carbon neutral energy economy where CO_2 emissions are captured and converted into fuels and other useful products.[1,2,9,15,16]

Electrochemical CO_2 conversion is a promising candidate for large-scale carbon management applications because it can operate with high reaction rates and good efficiency at ambient conditions.[5,7,8,10,13,14,17−19] A typical electrochemical system contains two electrically biased electrodes: CO_2 and protons are converted into products at the negatively charged cathode, and H_2O is oxidized into O_2 and protons at the positively charged anode. CO_2 can be converted into a variety of products,[5,18] and Table 1 summarizes the formal potentials (E^0) and number of protons and electrons associated with several common CO_2 reduction reaction (CO_2RR) products.[5] The total cell voltage required for CO_2RR includes potentials for both anodic and cathodic processes ($E_{cell} = E_{anode} - E_{cathode}$).[10] However, cell voltages often exceed the reaction formal potentials because real-world CO_2RR and oxygen evolution reaction (OER) catalysts require overpotentials of several hundred millivolts to achieve satisfactory reaction rates. At a process level these overpotentials represent wasted energy that can lead to inefficiencies including broad product distributions at the cathode, competitive H_2 evolution from proton reduction, and reduced Faradaic efficiencies (FE; Supporting Information eq S1).[2−7,19]

Received: May 20, 2015
Accepted: June 29, 2015
Published: June 29, 2015

DOI: 10.1021/acsami.5b04393
ACS Appl. Mater. Interfaces 2015, 7, 15626−15632

Table 1. Formal Potentials (E^0) Associated with the Electrochemical CO_2 Reduction Reaction (CO_2RR) and Oxygen Evolution Reaction (OER)[5,a]

electrode	reaction	E^0
cathode	$CO_2 + 2H^+ + 2e^- \rightarrow CO + H_2O$	−0.106
	$CO_2 + 2H^+ + 2e^- \rightarrow HCOOH$	−0.250
	$CO_2 + 4H^+ + 4e^- \rightarrow HCOH + H_2O$	−0.070
	$CO_2 + 6H^+ + 6e^- \rightarrow CH_3OH + H_2O$	0.016
	$CO_2 + 8H^+ + 8e^- \rightarrow CH_4 + 2H_2O$	0.169
	$CO_2 + 8H^+ + 12e^- \rightarrow C_2H_4 + 2H_2O$	0.064
	$2H^+ + 2e^- \rightarrow H_2$	0.000
anode	$2H_2O - 4e^- \rightarrow O_2 + 4H^+$	1.230

[a] All potentials are referenced against the reversible hydrogen electrode (RHE).

Carbon balance is an important consideration for electrochemical technologies because they require electricity to promote the CO_2RR. A simple analysis shows that carbon-free energy sources must be used in CO_2RR processes to produce a net reduction in CO_2 levels. Figure 1 presents the electrical input required to convert 1 metric tonne of CO_2 into various products (left axis) compared with the CO_2 produced from that amount of fossil-fuel-derived electricity (right axis). These calculations assume production rates of 0.6 kg_{CO_2}/kWh for fossil-fuel-derived electricity,[20] and the details for developing Figure 1 are contained in eqs S2−S5 and Tables S1 and S2 of the Supporting Information. The gray squares represent ideal CO_2RR and OER with zero overpotential and 100% FE. CO_2RR energy requirements scale linearly with the number of electrons involved in the reaction, and all fossil-fuel-powered reactions, except CO and HCOOH formation, produce more CO_2 than they consume.

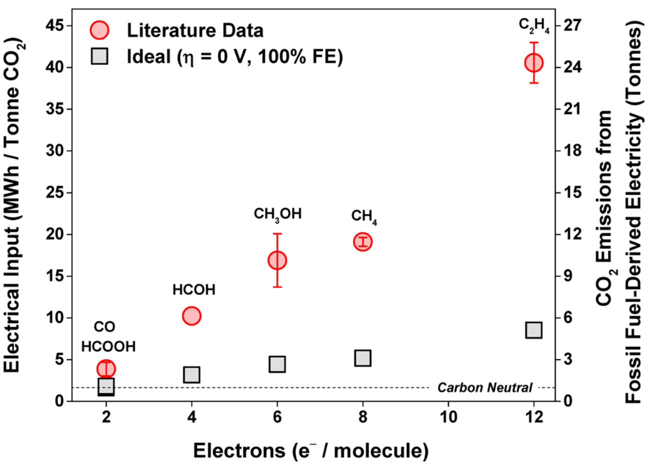

Figure 1. Electrical input required to convert 1 metric tonne of CO_2 into various products (left axis) compared with the CO_2 produced from that amount of fossil-fuel-derived electricity (right axis; 0.6 $kg_{CO_2}/kWh_{electricity}$).[20] Gray squares represent ideal CO_2 conversion at zero overpotential and 100% Faradaic efficiency. Red circles were calculated from literature examples of CO_2RR catalyst systems using the reported cathode voltage and FE and assuming 500 mV overpotential for OER (Supporting Information eqs S1−S4 and Tables S1 and S2).[2,5,6,13,14,18,21−33] These data identify that fossil-fuel-derived electricity is an impractical input for CO_2 conversion systems because it produces a net increase in CO_2 emissions; i.e., the processes are *carbon positive*.

Real catalyst systems require substantial CO_2RR and OER overpotentials and they typically operate at less than 100% FE. To account for this nonideality Figure 1 also presents electrochemical reaction data from selected catalyst systems in the literature.[2,5,6,13,14,18,21−33] We plotted these data using reported cathode voltages and FEs and we assumed a 500 mV overpotential for the OER (Supporting Information Table S2).[2] If a report listed multiple CO_2RR potentials, we chose conditions that maximized the reaction rate and FE. The overpotentials and FEs associated with real catalyst systems increase CO_2RR energy requirements so that all fossil-fuel-powered systems produce more CO_2 than they consume; i.e., they are carbon positive. Figure 1 illustrates that viable electrochemical CO_2 conversion technologies must integrate with carbon-free energy; however, very few reports have characterized renewably powered CO_2 conversion processes, the catalysts that can be utilized, or how these processes can be interfaced with carbon-friendly energy sources.[34−37]

This work describes the development and characterization of a renewably powered electrocatalytic CO_2 conversion system. We utilize ligand-protected $Au_{25}(SC_2H_4Ph)_{18}$ nanoclusters (abbreviated Au_{25}) as an extremely active and selective CO_2RR catalyst.[13,14] Previous work from our group has demonstrated that Au_{25} promotes the electrocatalytic conversion of CO_2 into CO with 98−99+% selectivity and FE in small, 15 mL batch reactors.[13,14] Real-world systems will require much larger, continuous flow reactors, and our current efforts focus on straightforward techniques for fabricating Au_{25}-containing electrodes and incorporating them into a simple, continuous flow system. High reaction rates, tunable product selectivity, and turnover numbers (TONs) between 1×10^6 and 4×10^6 mol_{CO_2} $mol_{catalyst}^{-1}$ were obtained with inexpensive ($10−20 USD), consumer-grade renewable-energy sources. In this regard, we are able to demonstrate a *carbon negative* CO_2 management technology because CO_2 is converted into CO without producing additional emissions from fossil-fuel-derived electricity. These results provide a proof-of-principle demonstration of a renewably powered CO_2 conversion process and some initial performance data needed to assess the scalability of this approach. Impressive catalyst performance with off-the-shelf, renewable-energy technology illustrates that current, state-of-the-art photovoltaic and battery technologies will be sufficient for larger CO_2 conversion applications.

■ RESULTS AND DISCUSSION

Optimizing Catalyst Loading and CO:H_2 Ratios. Our group[13] and others[33,38] have identified relationships between nanocatalyst loading and CO_2RR activity that must be characterized for developing CO_2 conversion processes. We also illustrate later that catalyst loading and dispersion can be exploited to tune CO:H_2 ratios in the product stream. Catalyst dispersion is an important parameter in heterogeneously catalyzed reactions, and well dispersed particles generally show higher surface area and better reactivity compared with poorly dispersed (aggregated) particles.[39] Several groups have extended this concept to electrochemical reactions,[40−45] and catalyst loading vs activity trends should be characterized to balance catalyst utilization and overall process rates.

We analyzed loading-dependent CO_2RR activity by depositing exact amounts of Au_{25} onto electrodes, and catalyst loadings are reported as the mass of Au *per* geometric electrode area (μg_{Au} cm_{geo}^{-2}). Specific experimental details are contained in

DOI: 10.1021/acsami.5b04393
ACS Appl. Mater. Interfaces 2015, 7, 15626−15632

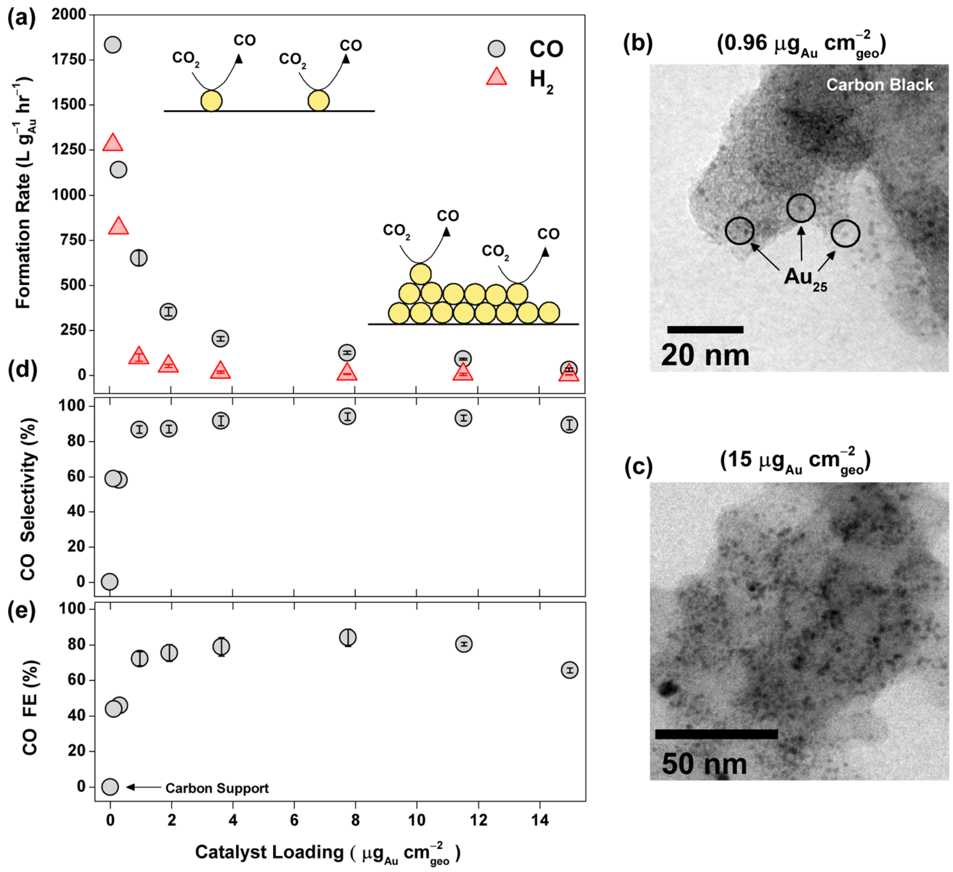

Figure 2. (a) Catalyst loading vs CO production rate for Au_{25} operated at −1 V vs RHE and a CO_2 flow rate of 20 mL min^{-1}. The inset of panel a contains a schematic describing reactant access to well dispersed and poorly dispersed catalyst particles. (b, c) TEM images of carbon-supported Au_{25} particles at low and high loadings. Isolated 1.4 ± 0.4 nm Au_{25} particles were observed on the carbon black support at low loadings. Both isolated Au_{25} particles and larger particle aggregates were observed at the higher catalyst loading. (d, e) CO selectivity and Faradaic efficiency (FE) as a function of catalyst loading. The carbon support evolved H_2 with >99% selectivity at −1 V vs RHE (Supporting Information Figure S2), and larger support-to-catalyst ratios in the low-loading regime decreased the CO selectivity and FE for Au_{25} catalysts. Error bars represent the standard deviation from three 1 h electrolysis runs.

the Supporting Information. Briefly, CO_2 was bubbled into the cathode compartment electrolyte (catholyte) at specific flow rates (mL min^{-1}) and a constant potential was applied to the Au_{25}-containing cathode with a potentiostat. The effluent gas stream was collected and the reaction products were analyzed every 30 min with gas chromatography. We report the product formation rates as liters of gas produced *per* gram Au *per* hour (L g_{Au}^{-1} h^{-1}), and FE values were calculated from the integrated electrolysis charge and the detected reaction products (Supporting Information eq S1).

Figure 2 summarizes the relationship between CO_2RR rate, product selectivity, FE, and catalyst loading at an applied potential of −1 V vs RHE and a CO_2 flow rate of 20 mL min^{-1}. Figure 2a shows higher CO formation rates are associated with lower catalyst loadings. In fact, we observed an approximate 130-fold increase in mass-normalized CO production rates when the catalyst loading was reduced from 15 to 0.1 μg_{Au} cm_{geo}^{-2}. The inset of Figure 2a describes our proposed mechanism for loading-dependent CO_2RR rates. Low catalyst loadings produce well dispersed, spatially separated Au_{25} catalysts that do not compete for incoming reactants.[40−45] This scenario produces high CO_2RR rates because reactants can easily access the Au_{25} surface and each particle can function as an isolated reaction center. Conversely, high catalyst loadings produce closely spaced particles and/or larger particle aggregates. These particles must compete for incoming reactant molecules, and the system shows lower mass-normalized CO_2RR rates. Transmission electron microscopy (TEM) supports this hypothesis, and we find well dispersed particles at lower catalyst loadings and aggregated particles at higher loadings (Figure 2b,c and Supporting Information Figure S1). The 1−2 nm size of apparently isolated Au_{25} particles is consistent with the expected particle size,[46−48] and previous work has shown the larger structures on high-loading electrodes represent closely spaced and/or aggregated Au_{25} particles, rather than larger Au nanocrystals.[13] We also observed increased H_2 evolution at low catalyst loadings (Figure 2d,e). The carbon electrode and carbon support evolve H_2 with >99% selectivity at −1 V vs RHE (Supporting Information Figure S2), and increased H_2 evolution occurs at low catalyst loadings because larger fractions of the carbon electrode and carbon support are exposed to solution.

We also point out that other parameters can adjust CO:H_2 ratios, reaction rates, and efficiencies. The electrode potential can also modify CO:H_2 ratios, and H_2 evolution becomes dominant at potentials more negative than −1.4 V (Supporting Information Figure S3). Finally, the rate at which CO_2 flows into the catholyte also influences catalytic activity, and higher CO_2 flow rates produced larger reaction rates, FEs, and product selectivity (Supporting Information Figure S4); however, this

DOI: 10.1021/acsami.5b04393
ACS Appl. Mater. Interfaces 2015, 7, 15626−15632

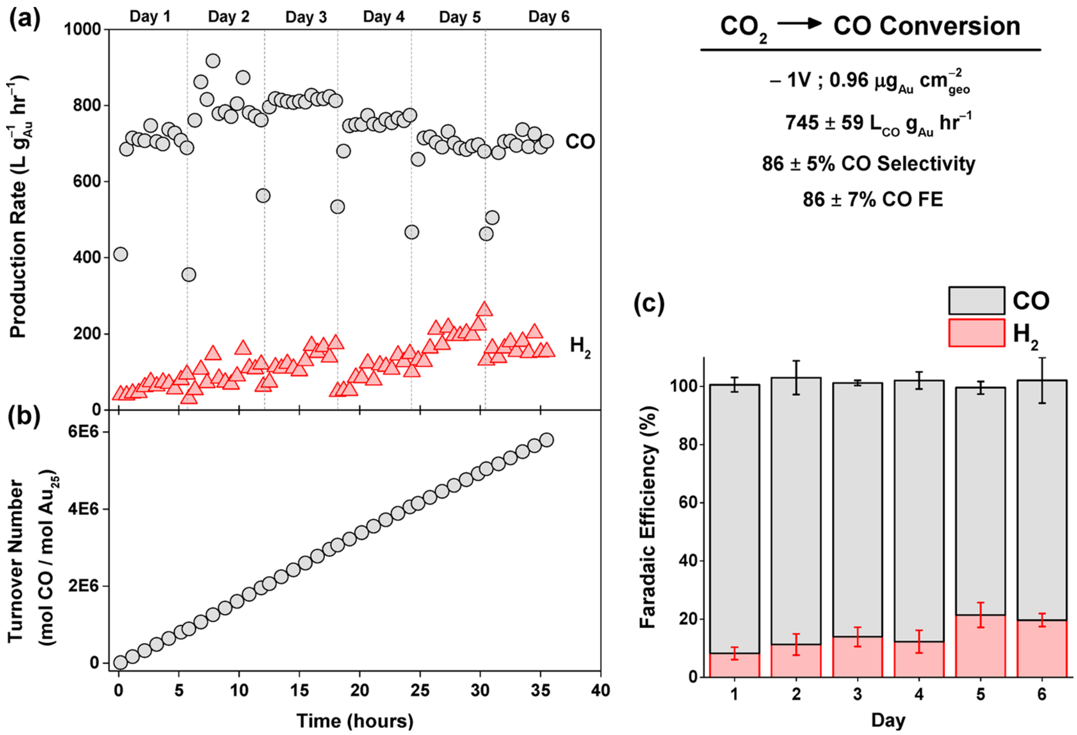

Figure 3. Day-to-day (a) product formation rates, (b) cumulative turnover number (TON, mol of CO/(mol of Au_{25})), and (c) Faradaic efficiency during a 36 h CO_2RR experiment. The electrode contained 0.96 μg_{Au} cm_{geo}^{-1}, it was operated at −1 V vs RHE, and CO_2 was bubbled into solution with a flow rate of 50 mL min^{-1}. Daily current vs time curves are presented in Supporting Information Figure S7.

effect was small beyond flow rates larger than 50 mL_{CO_2} min^{-1}. Based on the preceding data, we chose conditions that selectively produced CO, including a catalyst loading of 0.96 μg_{Au} cm_{geo}^{-2}, a cathode voltage of −1 V vs RHE, and a CO_2 flow rate of 50 mL min^{-1}. These conditions produced CO at 810 ± 11 L g_{Au}^{-1} h^{-1} with better than 90% CO selectivity and FE during 1 h electrolysis runs. We chose conditions that favored selective CO production to characterize maximum TOF, TON, and catalyst stability, but one could target other CO:H_2 ratios by simply adjusting the catalyst loading, operating voltage, and/or CO_2 flow rate as described previously. Efficient and tunable product formation will be important for scaled-up electrochemical CO_2RR because downstream conversion of CO and H_2 into CH_4, methanol, or Fischer−Tropsch products requires different CO:H_2 ratios.[21]

Long-Term Performance. We evaluated long-term CO_2RR performance at conditions favoring selective CO formation (0.96 μg_{Au} cm_{geo}^{-2}, −1 $V_{cathode}$; 50 mL_{CO_2} min^{-1}), and Figure 3 presents potentiostat-controlled CO_2RR over 6 days. The electrolysis was run for 5−6 h each day to mimic realistic, on-demand usage that is known to degrade catalysts and carbon electrodes in real-world applications such as fuel cells.[49] Gas samples were collected every 30 min, but we excluded the first daily samples from data analysis because our system required ~45 min to achieve steady state operation. We found average CO formation rates of 745 ± 59 L g_{Au}^{-1} h^{-1}, CO selectivities of 86 ± 5%, and CO FEs of 86 ± 7% during the long-term CO_2RR. We determined an average turnover frequency (TOF) of 46 ± 3 mol_{CO} $mol_{Au_{25}}^{-1}$ s^{-1}, a cumulative TON approaching 6×10^6 mol_{CO} $mol_{catalyst}^{-1}$, and an overall FE of 102 ± 6% accounting for both CO production and H_2 evolution. Postreaction TEM and XPS analysis showed some particle coarsening and binding energy shifts in the Au 4f and ligand S 2p spectral regions (Supporting Information Figures S5 and S6). Alivisatos and co-workers described the aggregation of ligand-free Au nanoparticles during CO_2 electrolysis,[50] and our results suggest ligand desorption allowed some particle sintering during extended electrolysis experiments. Ligand-free Au particles demonstrate lower CO selectivity,[51] and a combination of ligand desorption, particle sintering, and/or H_2 evolution from the carbon support may gradually reduce CO selectivity. However, this phenomenon may not present a significant problem in systems that operate at lower voltages and/or target H_2-rich CO:H_2 product streams.

Mass activity (A g^{-1}) is another metric that quantifies electrocatalytic current with respect to catalyst mass. Au_{25} demonstrated long-term CO_2RR mass activity of 1656 ± 163 A g_{Au}^{-1} based on the daily current (Supporting Information Figure S7), daily average CO FE (Figure 3c), and total Au loading (12.5 μg). Previous rotating disk electrode experiments produced Au_{25} mass activities approaching 3900 A g_{Au}^{-1} at −1 V vs RHE.[13] In the present case, slower reactant transport to the stationary planar electrodes likely reduced mass activity compared with RDE studies, and real-world systems would need to optimize the electrode geometry and solution agitation to maximize reaction rates. In comparison, Kenis and co-workers reported 2700 A g^{-1} for CO production at −0.8 V vs RHE with 1 cm^{-2} Ag/TiO_2-decorated gas diffusion electrodes,[38] Alivisatos and co-workers reported ~760 A g^{-1} for CH_4 production at −1.25 V vs RHE with 7 nm Cu nanoparticles,[33] we reported 20−60 A g^{-1} for CO production at −1.0 V vs RHE with sub-10 nm copper oxide nanoparticles,[24] and Peterson and co-workers reported 14 A g^{-1} for CO production at −0.9 V vs RHE with 4 nm Au NPs.[21] It is unclear if poor catalyst dispersion artificially decreased the performance of non-Au_{25} systems, and future electrocatalyst studies will need to evaluate

DOI: 10.1021/acsami.5b04393
ACS Appl. Mater. Interfaces 2015, 7, 15626−15632

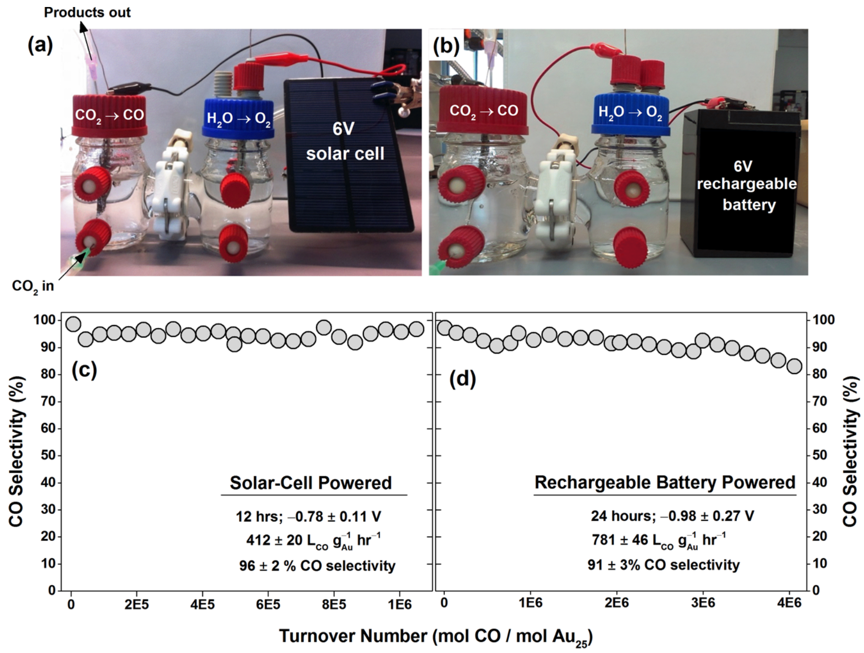

Figure 4. (a, b) Photographs of an electrochemical CO_2 reactor powered by inexpensive ($10−20 USD) solar panels and a solar-rechargeable battery. (c, d) $CO_2 \rightarrow CO$ selectivity as a function of turnover number when powered with a solar cell or solar-rechargeable battery (where, for example, 2E5 represents 2×10^5). The panels summarize operating time, average cathode voltage, CO production rate, and CO selectivity. Solar power operation mimics a 12 h sunny day, and battery-powered operation mimics nighttime hours, low-light conditions, or periods of unavailable renewable electricity. Supporting Information Figure S8 shows a photograph of the battery connected to the solar charger.

mass activity vs loading relationships when characterizing CO_2RR catalysts.

Renewable-Energy-Powered CO_2 Conversion. We have coupled our electrochemical reactor with inexpensive ($10−20 USD), consumer-grade renewable-energy sources to mimic day and nighttime operating conditions. Panels a and b of Figure 4 present photographs of the CO_2 reactor connected to a 1.5 W, 6 V solar panel and a solar-rechargeable 6 V battery. Solar-cell-powered CO_2RR was conducted for 12 h to mimic operation during a sunny day (6 h/day, 2 days). The solar cell provided −0.78 ± 0.11 V vs RHE to the cathode and +4.53 ± 0.04 V vs RHE to the Pt anode. Figure 4c summarizes the solar-powered CO_2RR operation with CO production rates of 412 ± 20 L_{CO} g_{Au}^{-1} h^{-1}, 96 ± 2% selectivity, and a cumulative TON exceeding 1×10^6 mol_{CO} $mol_{catalyst}^{-1}$. Battery banks can provide stable operation in the absence of renewable energy during nighttime hours or windless conditions. A solar-rechargeable 6 V battery provided −0.98 ± 0.27 V to the cathode and +5.49 ± 0.27 V to the anode (Supporting Information Figure S8). Figure 4d summarizes the battery-powered operation with a CO production rate of 781 ± 46 L_{CO} g_{Au}^{-1} h^{-1}, 91 ± 3% selectivity, and a cumulative TON exceeding 4×10^6 mol_{CO_2} $mol_{catalyst}^{-1}$ over 24 h of operation (6 h per day, 4 days). Incorporating electronics to individually control electrode potentials could reduce the anode overpotential and tune the cathodic reaction rate and product selectivity. High catalyst performance from commonly available renewable-energy power sources provides a compelling case that current, state-of-the-art renewable-energy technologies are sufficient to power industrial CO_2RR processes and that new photovoltaic and energy storage technologies are not needed to advance this process.

Estimates for Larger-Scale CO_2 Conversion Systems. The reaction rate, FE, and energy input data presented earlier enables us to make simple estimates of the process requirements and expected performance on larger scales. We acknowledge that many variables can impact the performance of a particular system, including batch vs continuous flow operation, electrolyte temperature, composition, concentration and pH, gas inlet and outlet pressures, interelectrode separation, and CO_2 residence time.[52−54] Some of these considerations are beyond the scope of this work; however, we can make performance estimates for larger-scale systems with metrics similar to our Au_{25}-based system. For example, a system with performance similar to Au_{25} operating with a cathodic voltage of −1 V, an anodic voltage of +1.73 V, and 87% FE would require 3.82 MWh to convert 1 metric tonne of CO_2 into CO (Supporting Information eqs S2−S5). Energy requirements will increase for more complex products and/or less efficient catalysts, but they are accessible with state-of-the-art renewable-energy technology. For example, solar installations can produce 3.9 MWh $acre^{-1}$ day^{-1} assuming a daily solar irradiance of 6 kWh m^{-2} and 16% photovoltaic efficiency.[2] Our experimental data provide an upper CO_2 conversion capacity of 1.0 tonne of CO_2 $acre^{-1}$ day^{-1} for photovoltaic-powered systems with performance similar to Au_{25}. A 1.0 MW wind turbine operating at 25% capacity could produce 6 MWh day^{-1}, and we estimate an upper CO_2 conversion capacity of 1.6 tonnes of CO_2 day^{-1} $turbine^{-1}$ for wind-powered CO_2 conversion systems with performance similar to Au_{25}. Other renewable power sources such as geothermal or hydroelectric power are also suitable energy inputs, and the United States produced approximately 4.8×10^8 MWh of electricity from noncombustible renewable-energy sources in 2014.[55] Utilizing 1% of the renewable energy currently produced in the United States could convert between 2.5×10^5 and 1.2×10^6 metric tonnes of CO_2 into CO, HCOH, CH_3OH, or CH_4 using the catalysts summarized in Figure 1. Installing dedicated renewable-energy sources would increase CO_2 capacity, and excess

DOI: 10.1021/acsami.5b04393
ACS Appl. Mater. Interfaces 2015, 7, 15626−15632

electricity could be fed back into the electrical grid to further reduce CO_2 emissions. These estimates show that tonne *per* day CO_2 conversion systems are feasible with current catalyst systems and renewable-energy sources.

■ CONCLUSIONS

Our estimates indicate that state-of-the-art renewable technologies are sufficient to power large-scale CO_2 conversion systems operating at tonne *per* day rates. We have shown that impressive catalytic reaction rates, product selectivities, and efficiencies can be achieved with off-the-shelf, consumer-grade renewable-energy sources. We expect other catalyst systems will show similarly impressive performance when coupled to renewable-energy sources, and our work highlights the potential for renewably powered electrochemical CO_2 conversion systems. The anode catalyst is another important aspect of CO_2 conversion because it consumes roughly half of the electrical input. Improving the anode efficiency and reducing OER overpotentials will decrease the overall energy requirements for CO_2 conversion and make this carbon mitigation strategy even more practical.

■ ASSOCIATED CONTENT

Ⓢ Supporting Information

Text containing experimental details, tables listing ideal energy requirements for CO_2 conversion and energy requirements for selected cataytic conversions, and figures showing SEM and TEM images, product formation rates, H_2 and CO selectivities, Faradaic efficiencies, XPS of Au 4f and S 2p regions, CO_2RR currents, and photograph of solar-rechargeable battery, . The Supporting Information is available free of charge on the ACS Publications website at DOI: 10.1021/acsami.5b04393.

■ AUTHOR INFORMATION

Corresponding Author

*E-mail: Douglas.Kauffman@NETL.DOE.GOV.

Notes

The authors declare no competing financial interest.

■ ACKNOWLEDGMENTS

R.J. acknowledges research support from AFOSR. This report was prepared as an account of work sponsored by an agency of the United States Government. Neither the United States Government nor any agency thereof, nor any of their employees, makes any warranty, express or implied, or assumes any legal liability or responsibility for the accuracy, completeness, or usefulness of any information, apparatus, product, or process disclosed, or represents that its use would not infringe privately owned rights.

■ REFERENCES

(1) Olah, G. A. Beyond Oil and Gas: The Methanol Economy. *Angew. Chem., Int. Ed.* **2005**, *44*, 2636−2369.

(2) Herron, J. A.; Kim, J.; Upadhye, A. A.; Huber, G. W.; Maravelias, C. T. A General Framework for the Assessment of Solar Fuel Technologies. *Energy Environ. Sci.* **2015**, *8*, 126−157.

(3) Schouten, K. J. P.; Calle-Vallejo, F.; Koper, M. T. M. A Step Closer to the Electrochemical Production of Liquid Fuels. *Angew. Chem., Int. Ed.* **2014**, *53*, 10858−10860.

(4) Ebbesen, S. D.; Jensen, S. H.; Hauch, A.; Mogensen, M. B. High Temperature Electrolysis in Alkaline Cells, Solid Proton Conducting Cells, and Solid Oxide Cells. *Chem. Rev.* **2014**, *114*, 10697−10734.

(5) Qiao, J.; Liu, Y.; Hong, F.; Zhang, J. A Review of Catalysts for the Electroreduction of Carbon Dioxide to Produce Low-Carbon Fuels. *Chem. Soc. Rev.* **2014**, *43*, 631−675.

(6) Peterson, A. A.; Nørskov, J. K. Activity Descriptors for CO_2 Electroreduction to Methane on Transition-Metal Catalysts. *J. Phys. Chem. Lett.* **2012**, *3*, 251−258.

(7) Kuhl, K. P.; Hatsukade, T.; Cave, E. R.; Abram, D. N.; Kibsgaard, J.; Jaramillo, T. F. Electrocatalytic Conversion of Carbon Dioxide to Methane and Methanol on Transition Metal Surfaces. *J. Am. Chem. Soc.* **2014**, *136*, 14107−14113.

(8) Whipple, D. T.; Kenis, P. J. A. Prospects of CO_2 Utilization *via* Direct Heterogeneous Electrochemical Reduction. *J. Phys. Chem. Lett.* **2010**, *1*, 3451−3458.

(9) Goeppert, A.; Czaun, M.; Jones, J.-P.; Prakash, G. K. S.; Olah, G. A. Recycling of Carbon Dioxide to Methanol and Derived Products − Closing the Loop. *Chem. Soc. Rev.* **2014**, *43*, 7995−8048.

(10) Jhong, H.-R. M.; Ma, S.; Kenis, P. J. A. Electrochemical Conversion of CO_2 to Useful Chemicals: Current Status, Remaining Challenges, and Future Opportunities. *Curr. Opin. Chem. Eng.* **2013**, *2*, 191−199.

(11) Centi, G.; Quadrelli, E. A.; Perathoner, S. Catalysis for CO_2 Conversion: A Key Technology for Rapid Introduction of Renewable Energy in the Value Chain of Chemical Industries. *Energy Environ. Sci.* **2013**, *6*, 1711−1731.

(12) Wang, C.; Ranasingh, O.; Natesakhawat, S.; Ohodnicki, P. R., Jr.; Andio, M.; Lewis, J. P.; Matrangaa, C. Visible Light Plasmonic Heating of Au−ZnO for the Catalytic Reduction of CO_2. *Nanoscale* **2013**, *5*, 6968−6974.

(13) Kauffman, D. R.; Alfonso, D.; Matranga, C.; Ohodnicki, P.; Deng, X.; Siva, R. C.; Zeng, C.; Jin, R. Probing active site chemistry with differently charged Au_{25}^{q} nanoclusters (q = −1, 0, +1). *Chem. Sci.* **2014**, *5*, 3151−3157.

(14) Kauffman, D. R.; Alfonso, D.; Matranga, C.; Qian, H.; Jin, R. Experimental and Computational Investigation of Au_{25} Clusters and CO_2: A Unique Interaction and Enhanced Electrocatalytic Activity. *J. Am. Chem. Soc.* **2012**, *134*, 10237−10243.

(15) Olah, G. A.; Goeppert, A.; Prakash, G. K. S. Chemical Recycling of Carbon Dioxide to Methanol and Dimethyl Ether: From Greenhouse Gas to Renewable, Environmentally Carbon Neutral Fuels and Synthetic Hydrocarbons. *J. Org. Chem.* **2009**, *74*, 487−498.

(16) Ozin, G. A. Throwing New Light on the Reduction of CO_2. *Adv. Mater.* **2015**, *27*, 1957−1963.

(17) Kuhl, K. P.; Cave, E. R.; Abram, D. N.; Jaramillo, T. F. New Insights Into the Electrochemical Reduction of Carbon Dioxide on Metallic Copper Surfaces. *Energy Environ. Sci.* **2012**, *5*, 7050−7059.

(18) Gattrell, M.; Gupta, N.; Co, A. A Review of the Aqueous Electrochemical Reduction of CO_2 to Hydrocarbons at Copper. *J. Electroanal. Chem.* **2006**, *594*, 1−19.

(19) Hansen, H. A.; Varley, J. B.; Peterson, A. A.; Nørskov, J. K. Understanding Trends in the Electrocatalytic Activity of Metals and Enzymes for CO_2 Reduction to CO. *J. Phys. Chem. Lett.* **2013**, *4*, 388−392.

(20) *The Emissions & Generation Resource Integrated Database (eGRID)*, 9th ed.; U.S. Environmental Protection Agency, Washington, DC, USA, 2014; http://www.epa.gov/cleanenergy/energy-resources/egrid/index.html.

(21) Zhu, W.; Michalsky, R.; Metin, O. n.; Lv, H.; Guo, S.; Wright, C. J.; Sun, X.; Peterson, A. A.; Sun, S. Monodisperse Au Nanoparticles for Selective Electrocatalytic Reduction of CO_2 to CO. *J. Am. Chem. Soc.* **2013**, *135*, 16833−16836.

(22) Zhu, W.; Zhang, Y.-J.; Zhang, H.; Lv, H.; Li, Q.; Michalsky, R.; Peterson, A. A.; Sun, S. Active and Selective Conversion of CO_2 to CO on Ultrathin Au Nanowires. *J. Am. Chem. Soc.* **2014**, *136*, 16132−16135.

(23) Chen, Y.; Li, C. W.; Kanan, M. W. Aqueous CO_2 Reduction at Very Low Overpotential on Oxide-Derived Au Nanoparticles. *J. Am. Chem. Soc.* **2012**, *134*, 19969−19972.

(24) Kauffman, D. R.; Ohodnicki, P. R.; Kail, B. W.; Matranga, C. Selective Electrocatalytic Activity of Ligand Stabilized Copper Oxide Nanoparticles.pdf. *J. Phys. Chem. Lett.* **2011**, *2*, 2038−2043.

(25) Rosen, B. A.; Salehi-Khojin, A.; Thorson, M. R.; Zhu, W.; Whipple, D. T.; Kenis, P. J. A.; Masel, R. I. Ionic Liquid-Mediated Selective Conversion of CO_2 to CO at Low Potentials. *Science* **2011**, *334*, 643−644.

(26) Tornow, C. E.; Thorson, M. R.; Ma, S.; Gewirth, A. A.; Kenis, P. J. A. Nitrogen-Based Catalysts for the Electrochemical Reduction of CO_2 to CO. *J. Am. Chem. Soc.* **2012**, *134*, 19520−19523.

(27) Li, C. W.; Kanan, M. W. CO_2 Reduction at Low Overpotential on Cu Electrodes Resulting from the Reduction of Thick Cu_2O Films. *J. Am. Chem. Soc.* **2012**, *134*, 7231−7234.

(28) Chen, Y.; Kanan, M. W. Tin Oxide Dependence of the CO2 Reduction Efficiency on Tin Electrodes and Enhanced Activity for Tin/Tin Oxide Thin-Film Catalysts. *J. Am. Chem. Soc.* **2012**, *134*, 1986−1989.

(29) Lee, C. H.; Kanan, M. W. Controlling H^+ *vs* CO_2 Reduction Selectivity on Pb Electrodes. *ACS Catal.* **2015**, *5*, 465−469.

(30) Zhang, S.; Kang, P.; Meyer, T. J. Nanostructured Tin Catalysts for Selective Electrochemical Reduction of Carbon Dioxide to Formate. *J. Am. Chem. Soc.* **2014**, *136*, 1734−1737.

(31) Zhang, S.; Kang, P.; Ubnoske, S.; Brennaman, M. K.; Song, N.; House, R. L.; Glass, J. T.; Meyer, T. J. Polyethylenimine-Enhanced Electrocatalytic Reduction of CO_2 to Formate at Nitrogen-Doped Carbon Nanomaterials. *J. Am. Chem. Soc.* **2014**, *136*, 7845−7848.

(32) Nakata, K.; Ozaki, T.; Terashima, C.; Fujishima, A.; Einaga, Y. High-Yield Electrochemical Production of Formaldehyde from CO_2 and Seawater. *Angew. Chem., Int. Ed.* **2014**, *53*, 871−874.

(33) Manthiram, K.; Beberwyck, B. J.; Alivisatos, A. P. Enhanced Electrochemical Methanation of Carbon Dioxide with a Dispersible Nanoscale Copper Catalyst. *J. Am. Chem. Soc.* **2014**, *136*, 13319−13325.

(34) Ogura, K.; Yoshida, I. Catalytic Conversion of CO and CO_2 into Methanol with a Solar Cell. *J. Mol. Catal.* **1986**, *34*, 309−311.

(35) Ogura, K.; Yoshida, I. Electrocatalytic Reduction of Carbon Dioxide to Methaol –VI. Use of a Solar Cell and Comparison with that of Carbon Monoxide. *Electrochim. Acta* **1987**, *32*, 1191−1195.

(36) White, J. L.; Herb, J. T.; Kaczur, J. J.; Majsztrik, P. W.; Bocarsly, A. B. Photons to Formate: Efficient Electrochemical Solar Energy Conversion *via* Reduction of Carbon Dioxide. *J. CO_2 Util.* **2014**, *7*, 1−5.

(37) Peng, Y. P.; Yeh, Y. T.; Wang, P. Y.; Huang, C. P. A Solar Cell Driven Electrochemical Process for the Concurrent Reduction of Carbon Dioxide and Degradation of Azo Dye in Dilute $KHCO_3$ Electrolyte. *Sep. Purif. Technol.* **2013**, *117*, 3−11.

(38) Ma, S.; Lan, Y.; Perez, G. M. J.; Moniri, S.; Kenis, P. J. A. Silver Supported on Titania as an Active Catalyst for Electrochemical Carbon Dioxide Reduction. *ChemSusChem* **2014**, *7*, 866−874.

(39) Sinfelt, J. H. Highly Dispersed Catalytic Materials. *Annu. Rev. Mater. Sci.* **1972**, *2*, 641−662.

(40) Bard, A. J.; Crayston, J. A.; Kittlesen, G. P.; Shea, T. V.; Wrighton, M. S. Digital Simulation of the Measured Electrochemical Response of Reversible Redox Couples at Microelectrode Arrays: Consequences Arising from Closely Spaced Ultramicroelectrodes. *Anal. Chem.* **1986**, *58*, 2321−2331.

(41) Watanabe, M.; Sei, H.; Stonehart, P. The influence of platinum crystallite size on the electroreduction of oxygen. *J. Electroanal. Chem. Interfacial Electrochem.* **1989**, *261*, 375−387.

(42) Streeter, I.; Baron, R.; Compton, R. G. Voltammetry at Nanoparticle and Microparticle Modified Electrodes: Theory and Experiment. *J. Phys. Chem. C* **2007**, *111*, 17008−17014.

(43) Seidel, Y. E.; Schneider, A.; Jusys, Z.; Wickman, B.; Kasemo, B.; Behm, R. J. Mesoscopic mass transport effects in electrocatalytic processes. *Faraday Discuss.* **2009**, *140*, 167−184.

(44) Belding, S. R.; Compton, R. G. Transient Voltammetry at Electrodes Modified with a Random Array of Spherical Nanoparticles: Theory. *J. Phys. Chem. C* **2010**, *114*, 8309−8319.

(45) Alia, S. M.; Larsen, B. A.; Pylypenko, S.; Cullen, D. A.; Diercks, D. R.; Neyerlin, K. C.; Kocha, S. S.; Pivovar, B. S. Platinum-Coated Nickel Nanowires as Oxygen-Reducing Electrocatalysts. *ACS Catal.* **2014**, *4*, 1114−1119.

(46) Akola, J.; Walter, M.; Whetten, R. L.; Häkkinen, H.; Grönbeck, K. On the Structure of Thiolate-Protected Au_{25}. *J. Am. Chem. Soc.* **2008**, *130*, 3756−3757.

(47) Zhu, M.; Aikens, C. M.; Hollander, F. J.; Schatz, G. C.; Jin, R. Correlating the Crystal Structure of a Thiol-Protected Au_{25} Cluster and Optical Properties. *J. Am. Chem. Soc.* **2008**, *130*, 5883−5885.

(48) Heaven, M. W.; Dass, A.; White, P. S.; Holt, K. M.; Murray, R. W. Crystal Structure of the Gold Nanoparticle $[N(C_8H_{17})_4]$-$[Au_{25}(SCH_2CH_2Ph)_{18}]$. *J. Am. Chem. Soc.* **2008**, *130*, 3754−3755.

(49) Wu, J.; Yuan, X. Z.; Martin, J. J.; Wang, H.; Zhang, J.; Shen, J.; Wu, S.; Merida, W. A Review of PEM Fuel Cell Durability: Degradation Mechanisms and Mitigation Strategies. *J. Power Sources* **2008**, *184*, 104−119.

(50) Manthiram, K.; Surendranath, Y.; Alivisatos, A. P. Dendritic Assembly of Gold Nanoparticles during Fuel-Forming Electrocatalysis. *J. Am. Chem. Soc.* **2014**, *136*, 7237−7240.

(51) Mistry, H.; Reske, R.; Zeng, Z.; Zhao, Z.-J.; Greeley, J.; Strasser, P.; Cuenya, B. R. Exceptional Size-Dependent Activity Enhancement in the Electroreduction of CO_2 over Au Nanoparticles. *J. Am. Chem. Soc.* **2014**, *136*, 16473−16476.

(52) Li, H.; Oloman, C. Development of a Continuous Reactor for the Electro-Reduction of Carbon Dioxide to Formate – Part 2: Scale-up. *J. Appl. Electrochem.* **2007**, *37*, 1107−1117.

(53) Jüttner, K., Technical Scale of Electrochemistry. In *Encyclopedia of Electrochemistry*; Bard, A. J.; Stratmann, M., Eds. Wiley-VCH Verlag GmbH: Weinheim, Germany, 2007; Vol. *5*, DOI: 10.1002/9783527610426.bard050001.

(54) Sulaymon, A. H.; Abbar, A. H. Electrochemical Reactors. In *Electrolysis*; Kleperis, J., Ed. InTech: Rijeka, Croatia, 2012; DOI: 10.5772/48728.

(55) Hankey, R.; Cassar, C.; Peterson, R.; Wong, P.; Knaub, J. *Electric Power Monthly*; U.S. Energy Information Administration, U.S. Department of Energy, Washington, DC, USA, February 2015; http://www.eia.gov/electricity/monthly/, Table 1.1A.

DOI: 10.1021/acsami.5b04393
ACS Appl. Mater. Interfaces 2015, 7, 15626−15632